Publication VIII

E. Tölö and A. Harju. 2010. Reduced density-matrix functional theory in quantum Hall systems. Physical Review B, volume 81, number 7, 075321, 12 pages.

Reduced density-matrix functional theory in quantum Hall systems

E. Tölö and A. Harju
Helsinki Institute of Physics and Department of Applied Physics, Aalto University, FI-02150 Espoo, Finland
(Received 16 December 2009; revised manuscript received 3 February 2010; published 25 February 2010)

We apply reduced density-matrix functional theory to the parabolically confined quantum Hall droplet in the spin-frozen strong magnetic field regime. One-body reduced density-matrix functional method performs remarkably well in obtaining ground states, energies, and observables derivable from the one-body reduced density matrix for a wide range of system sizes. At the strongly correlated regime, the results go well beyond what can be obtained with the density-functional theory. However, some of the detailed properties of the system, such as the edge Green's function, are not produced correctly unless we use the much heavier two-body reduced density-matrix method.

DOI: 10.1103/PhysRevB.81.075321 PACS number(s): 73.43.−f, 71.27.+a, 73.21.La

I. INTRODUCTION

Quantum Hall fluids occur at low temperature in clean two-dimensional electron systems exposed to a perpendicular magnetic field.[1,2] Different phases are characterized by the number ν that tells the ratio of the number of electrons to the number of single-particle states in a highly degenerate Landau level (the number of flux quanta piercing the sample). Near certain fractional filling factors ν, the interactions between electrons induce an energy gap and lead to a ground state with topological order manifest in exotic quasiparticles and non-Fermi-liquid edge modes.[3–11]

Straight from the outset, numerical simulations have been an indispensable guide in development of the theory.[4] While majority of the numerics are exact diagonalization studies only viable with small electron numbers, variational Monte Carlo[12] and density-functional theory[13,14] (DFT) have also been applied to larger systems. For example, accurate wave functions incorporating the complex nonperturbative effects of electron interactions have been theoretically devised and later backed up by the high overlap with exact numerical results for small systems. Due to such developments, reason behind the energy gap of simplest of the many fractions is now well understood within the framework of composite-fermion theory that allows for explicit construction of the many-body wave function and calculation of topological quantum numbers.[8] However, in going beyond the composite-fermion theory to more complex phases, the Monte Carlo method is crippled since a trustworthy trial wave function for the phases we would be interested to know more about is not known. In addition, owing to the strong correlations, the DFT is inaccurate at, for example, the paradigm fractional quantum Hall state at filling fraction $\nu=1/3$ where the vortices supposed to form a bound state with the electrons localize at fixed positions instead.[15] Consequently, the exact diagonalization is frequently the only viable alternative, leaving the large electron numbers beyond the reach of direct calculations, though the density-matrix renormalization-group method has brought some progress making a bit larger systems computationally feasible.[16,17]

During the past ten years, reduced density-matrix functional theory has been revived and applied successfully in the chemical physics community.[18–20] The method is known to handle, e.g., molecular dissociation limits better than standard DFT (Refs. 21 and 22) and it has recently been applied to homogeneous electron gas.[23,24] In this manuscript, we aim to probe the potential of the one-body reduced density-matrix functional theory (1-RDMFT) in a fractional quantum Hall system, specifically a parabolically confined quantum dot in the spin-frozen strong magnetic field regime. In contrast to many molecular and atomic systems where the dominant occupation numbers are typically close to one, this is a highly demanding application for any numerical method as fractional quantum Hall states have long-range quantum entanglement with all the occupation numbers small for example near 1/3 in the $\nu=1/3$ state.

The performance of various functionals in predicting ground states, energies, and observables attainable by the reduced density matrix is compared for small system to the exact diagonalization and Hartree-Fock (HF) with and without the Brillouin-Wigner (BW) perturbation theory. For larger systems with tens of particles, the comparison is done utilizing the accurate Laughlin wave function[4] for filling fraction $\nu=1/3$ state and Monte Carlo methods (MC). Energies are produced quite well in all systems at the strong-correlation regime $\nu \ll 1$. Even the bulk densities appear reasonably good and reproduce the predicted edge stripe phase.[25] However, we are still dealing with an approximate method that has its limitations. Detailed properties of the edge of the electron droplet, such as the edge tunneling exponent,[26,27] are not produced correctly by the present functionals.

For this reason, we also perform a small comparison with the heavier two-body reduced density-matrix functional theory[28] (2-RDMFT) (see the closely related work in Ref. 29). Including the exact electron interaction by the two-body reduced density-matrix functional appears to facilitate a more accurate description of the edge, however with a computational cost in large systems beyond the reach of present day computers.

The rest of the manuscript is organized as follows. In the next section, we briefly introduce the idea of reduced density-matrix functional methods. In Sec. III, we describe the model system and derive an exact formula for the energy contribution due to one-body operators present in our Hamiltonian such that only the interaction energy remains to be solved. Secs. IV A and IV B present the details of our

1-RDMFT and 2-RDMFT implementations, respectively. The 1-RDMFT results are divided according to the small or large size of the system into Secs. V A and V B, followed by the 2-RDMFT calculation in Sec. V C. Conclusions and future prospects are found in Sec. VI.

II. REDUCED DENSITY-MATRIX FUNCTIONAL THEORIES

The 1-RDMFT is based on the Gilbert's theorem, which guarantees that the ground-state expectation value of any observable is a unique functional of the 1-RDM γ.[30] It follows that the ground-state energy can be written as

$$F(\gamma) = \int_{\mathbb{R}^{2d}} d\mathbf{r}d\mathbf{r}'\,\delta(\mathbf{r}-\mathbf{r}')[T(\mathbf{r})+U(\mathbf{r})]\gamma(\mathbf{r},\mathbf{r}') + V_{\mathrm{ee}}(\gamma), \tag{1}$$

where T and U are the standard operators for the kinetic energy and an external potential while the functional for the interaction energy $V_{\mathrm{ee}}[\gamma]$ is unknown. It is simple to show that this functional yields the exact ground-state energy for the exact 1-RDM

$$\gamma(\mathbf{r},\mathbf{r}') = N\int \Psi^*(\mathbf{r},\mathbf{r}_2,\mathbf{r}_3,\ldots,\mathbf{r}_N) \times \Psi(\mathbf{r}',\mathbf{r}_2,\mathbf{r}_3,\ldots,\mathbf{r}_N)d\mathbf{r}_2 d\mathbf{r}_3\ldots d\mathbf{r}_N \tag{2}$$

if V_{ee} is replaced by half the Coulomb energy of the exact pair density

$$E_{ee} = \frac{e^2}{2\epsilon}\int_{\mathbb{R}^{2d}} d\mathbf{r}d\mathbf{r}'\frac{\rho_2(\mathbf{r},\mathbf{r}')}{|\mathbf{r}-\mathbf{r}'|},$$

$$\rho_2(\mathbf{r},\mathbf{r}') = N(N-1)\int \Psi^*(\mathbf{r},\mathbf{r}',\mathbf{r}_3,\ldots,\mathbf{r}_N) \times \Psi(\mathbf{r},\mathbf{r}',\mathbf{r}_3,\ldots,\mathbf{r}_N)d\mathbf{r}_3\ldots d\mathbf{r}_N. \tag{3}$$

The 2-RDMFT minimizes the resulting exact functional F subject to a subset of complete N-representability conditions, known as the two-representability conditions, and other possible constraints due to additional symmetries (see Sec. IV B). On the other hand, the crux of the 1-RDMFT is to approximate the pair density by a functional of the 1-RDM.[31] The customary way to do the approximation, which we will also employ in this paper, is to replace the pair density above by

$$\rho(\mathbf{r})\rho(\mathbf{r}') - \sum_{i,j} f(n_i,n_j)\phi_i^*(\mathbf{r})\phi_j^*(\mathbf{r}')\phi_j(\mathbf{r})\phi_i(\mathbf{r}'), \tag{4}$$

where $\rho(\mathbf{r})=\gamma(\mathbf{r},\mathbf{r})$ is the density at $\mathbf{r}$, ϕ_i are the natural orbitals (eigenvectors of γ), and f is a function solely of the natural occupation numbers $n_i\in[0,1]$ (eigenvalues of γ). The functional for the interaction energy in Eq. (1) then reads

TABLE I. Functions $f(n_i,n_j)$. S and W refer to the strongly and weakly occupied natural orbitals, respectively.

	$f(n_i,n_i)$	$f(n_i,n_{j\neq i})$
MU	n_i	$\sqrt{n_i n_j}$
GU	n_i^2	
MU-α	n_i	
GU-α	n_i^2	$(n_i n_j)^\alpha$
P-α	$n_i^{2\alpha}$	
BBC1	n_i	$\begin{cases} -\sqrt{n_i n_j} & i,j\in W \\ \sqrt{n_i n_j} & i,j\notin W \end{cases}$
BBC1S	n_i^2	
BBC2	n_i	$\begin{cases} -\sqrt{n_i n_j} & i,j\in W \\ n_i n_j & i,j\in S \\ \sqrt{n_i n_j} & \text{else} \end{cases}$
BBC2S	n_i^2	

$$V_{\mathrm{ee}}[\gamma] = \frac{e^2}{2\epsilon}\left[\int_{\mathbb{R}^{2d}} d\mathbf{r}d\mathbf{r}'\frac{\rho(\mathbf{r})\rho(\mathbf{r}')}{|\mathbf{r}-\mathbf{r}'|} - \sum_{i,j} f(n_i,n_j) \times \int_{\mathbb{R}^{2d}} d\mathbf{r}d\mathbf{r}'\frac{\phi_i^*(\mathbf{r})\phi_j^*(\mathbf{r}')\phi_j(\mathbf{r})\phi_i(\mathbf{r}')}{|\mathbf{r}-\mathbf{r}'|}\right]. \tag{5}$$

The form of f could vary in different type of systems, whereas those used in this study are enlisted in Table I in Sec. IV A. In analogy with the density-functional theory, the first term is referred to as the Hartree term while the latter is the exchange-correlation term. However, compared to the DFT, 1-RDMFT has a couple of advantages. First, the method obtains not only the density but the whole 1-RDM so that the ground-state expectation value of any one-body observable can be readily computed. Thus, for example kinetic and interaction energies can be readily separated and Green's functions calculated. Second, although both methods are, in principle, exact for an exact functional, due to the variable γ (vs. ρ), it is easier to develop a good 1-RDM functional than a good density functional. This is the reason why the DFT does not work in the strongly correlated regime where the proper treatment of electronic correlations is important. However, there are fresh ideas of how to treat strongly correlated electrons with DFT.[32,33]

III. QUANTUM-DOT MODEL

The quantum Hall droplet is modeled by the two-dimensional effective-mass Hamiltonian

$$H = \sum_{i=1}^{N}\left[\frac{\left(\mathbf{p}_i+\frac{e}{c}\mathbf{A}_i\right)^2}{2m^*} + \frac{m^*\omega_0^2 r^2}{2}\right] + \sum_{i<j}\frac{e^2}{\epsilon r_{ij}}, \tag{6}$$

where N is the number of electrons, $\mathbf{A}$ is the planar vector potential of the homogeneous magnetic field $\mathbf{B}$ perpendicular to the sample plane, and the energy scale of the external

confinement potential $\hbar\omega_0$ is typically a few meVs. The material parameters are the effective mass of the electrons $m^*=0.067m_e$ and the dielectric constant of the GaAs semiconductor medium $\epsilon=12.7$. Coulomb interactions tend to spontaneously polarize the electron spins in an effect known as quantum Hall ferromagnetism. For this reason, the relatively weak Zeeman term has been omitted and the electrons are assumed spin polarized. From here on, we use oscillator units so that the energies are expressed in units of $\hbar\omega$ and lengths in units of $\sqrt{\hbar/m^*\omega}$ where $\omega^2=\omega_0^2+(\omega_c/2)^2$ with cyclotron frequency $\omega_c=eB/m^*c$.

For $N=1$, the energy states are written as

$$\psi_n^m(z)=\sqrt{\frac{n!}{\pi(n+m)!}}z^m L_n^m(z\bar{z})e^{-z\bar{z}/2},\quad m\geq -n, n\geq 0 \tag{7}$$

where $z=x+iy$ and L_n^m are the generalized Laguerre polynomials. The corresponding eigenvalues are given by

$$E_n^m=2n+1+\left(1-\frac{\hbar\omega_c}{2}\right)m. \tag{8}$$

We take on interest in developing a computational method for the fractional quantum Hall states at the strong magnetic field regime so we may assume that $\omega_0\ll\omega_c$. Then $\hbar\omega_c/2$ is close to unity, such that the term in parentheses in Eq. (8) becomes small and values of quantum number n other than 0 become irrelevant to the low-energy physics. This is the Landau level projection to the band with $n=0$. It should not be difficult to generalize the 1-RDMFT method to include spin and several Landau levels and study the region $\nu>1$ as well, however, for simplicity we stick to the spin-polarized lowest Landau level $\nu\leq 1$ in this study.

Note that in our two-dimensional model, m in Eq. (7) is the one and only angular momentum quantum number. We can write the contribution to the total energy due to terms other than the Coulomb interaction for a system of N electrons in the lowest Landau level $n=0$ in terms of the total angular momentum (quantum number) M exactly as

$$T+U=\sum_{i=1}^{N}\left[1+\left(1-\frac{\hbar\omega_c}{2}\right)m_i\right]=N+\left(1-\frac{\hbar\omega_c}{2}\right)M. \tag{9}$$

As the total angular momentum operator $\hat{M}$ commutes with the total Coulomb interaction energy operator V_{ee}, to solve the Landau-level-projected spectrum, the remaining task is to find the common eigenstates of the Landau-level-projected V_{ee} and $\hat{M}$.

For N and M small enough, these are solved exactly with the configuration interaction (CI) method (exact diagonalization) since the number of possible single-particle states is finite. We may go to a bit larger N and M by taking interest in only the ground state and finding it by the Lanczos algorithm (cf. Refs. 34 and 35). However, the exponential growth of the many-body basis limits the particle number to around ten depending on M and some kind of an approximate calculation method becomes necessary. The Kohn-Sham DFT is still a good method for the weakly correlated regime[36] but for larger M the natural occupations tend far from 1 and the DFT no longer gives us good results. Absence of a reliable trial wave function for generic M makes the implementation of variational Monte Carlo rather uncertain.[12,37] In this paper we are going to see, if the reduced density-matrix functional theory can make itself useful. The expectation is that it will work better than DFT at least when the eigenvalues of the density matrix are small meaning $\nu\ll 1$. With several Landau levels, this would correspond to the situation where the highest-occupied Landau level has low filling fraction.

IV. COMPUTATIONAL METHODS

A. 1-RDMFT

Due to the exact formula for the one-body operators' energy contribution [Eq. (9)], the energy functional of Eq. (1) simplifies to

$$F[\gamma]=N+\left(1-\frac{\hbar\omega_c}{2}\right)M+V_{\mathrm{ee}}[\gamma] \tag{10}$$

with the constraints that the particle number and the total angular momentum are N and M, respectively. Moreover, the natural orbitals for energy state $|\Psi\rangle$ in the lowest Landau level are directly the single-particle energy states since the angular momentum conservation yields a diagonal density matrix in this basis

$$\gamma_{mm'}=\langle\Psi|a_m^\dagger a_{m'}|\Psi\rangle=\delta_{mm'}n_m, \tag{11}$$

where a_m and its adjoint annihilate and create a particle with quantum numbers $n=0$ and m [see Eq. (7)]. As $N-1$ particles have at least a total angular momentum $(N-1)(N-2)/2$, the maximum single-particle angular momentum becomes $k=M-(N-1)(N-2)/2$. Therefore, the minimization of the interaction energy reduces to the constrained minimization of a function whose variables are $k+1$ occupation numbers

$$V_{\mathrm{ee}}(\{n_i\}_{i=0}^k)=\frac{1}{2}\sum_{i,j}(n_i n_j V_{ijij}-f(n_i,n_j)V_{ijji}), \tag{12}$$

where V_{ijkl} are the interaction matrix elements of the lowest Landau level orbitals computed in Ref. 38 and the constraints are explicitly written as

$$\sum_{m=0}^{k}n_m=N\quad\text{and}\quad\sum_{m=0}^{k}n_m m=M. \tag{13}$$

To optimize the occupation numbers, we first express them in terms of variables θ_i such that $n_i=\sin^2\theta_i$. The minimization of V_{ee} with the above two remaining constraints is then performed with the interior point or Nelder-Mead algorithm of MATHEMATICA.[39]

A vast number of functions $f(n_i,n_j)$ have been proposed in the literature in treatment of simple atoms and molecules, and it is not immediately clear, which of them would work well in the current system. Table I summarizes those used in this work for small systems to find out the optimal ones. For large systems, we only use the density-matrix power functional $f(n_i,n_j)=(n_i,n_j)^\alpha$ (P-α).[24] Each form of the off-diagonal $f(n_i,n_{j\neq i})$ corresponds to two different functions,

first of which has diagonal $f(n_i,n_i)=n_i$ while the second has $f(n_i,n_i)=n_i^2$. Since the natural orbitals are orthonormal, integration of the approximate pair density in Eq. (4) over the coordinates yields the proper normalization $N(N-1)$ for $f(n_i,n_i)=n_i$. The form n_i^2, on the other hand, is justified as it cancels the self-interaction terms V_{iiii} arising from the Hartree term.

A few words about different forms of the off-diagonal terms are in order (see last column in Table I). The form $n_i^\alpha n_j^{1-\alpha}$ for f was first introduced by Müller (MU), who found $\alpha=1/2$ to be the optimal value.[18] Goedecker and Umrigar[40] (GU) used the modification to the diagonal that removes the self-interaction terms. Much similar to the density-matrix power functional, we generalize these to MU-α and GU-α where the square root is replaced by an arbitrary power, presumably lying between half and one. Alternatively, it is often physically motivated to reduce the overcorrelation of MU by switching the sign of the off-diagonal terms between weakly occupied natural orbitals W (BBC1) or additionally banishing the square root for pairs of strongly occupied orbitals S (BBC2).[22,23] For simplicity, we define the strongly and weakly occupied orbitals directly from the Hartree-Fock solution where the occupations are 0 or 1.

Finally, we would like to point out an issue with the physicality of the obtained solution, which is generally more of a problem in the higher-order RDM methods. Specifically, Coleman has shown that necessary and sufficient condition for the 1-RDM to be N representable, meaning that there exists $|\Psi\rangle$ in the Hilbert space of the system such that $\gamma_{ij}=\langle\Psi|a_i^\dagger a_j|\Psi\rangle$, is that its eigenvalues are between 0 and 1 and their sum is N.[41] However, if we additionally demand a symmetry, it may be that the obtained solution is not representable in the symmetry-restricted part of the Hilbert space. To be explicit, if in our model we demand total angular momentum of a two electron system to be 2, the symmetry-restricted Hilbert space of states with $m=0$, 1, and 2 consists only of one state with occupations (1,0,1) while 1-RDM method could give us unphysical occupations (0.5,1,0.5) both having the same particle number and angular momentum $(0.5\times0+1\times1+0.5\times2=2)$. While this could be avoided by imposing additional constraints, we refrain from doing it as that would be exponentially unfeasible for larger systems. Additionally, it is plausible that the unphysical solutions have less weight when the size of the physical Hilbert space increases.

B. 2-RDMFT

In analogy with the 1-RDMFT, we now minimize a functional of the 2-RDM

$$\Gamma_{kl}^{ij}=\langle\Psi|a_i^\dagger a_j^\dagger a_l a_k|\Psi\rangle. \tag{14}$$

The marked difference is that we now have an exact functional for the interaction energy

$$V_{\mathrm{ee}}(\Gamma)=\frac{1}{2}\sum_{i,j,k,l}\Gamma_{kl}^{ij}V_{ijkl} \tag{15}$$

however, with the cost of large number of additional parameters to optimize with similarly large number of additional constraints. Furthermore, the set of constraints to be listed below form a relatively stringent set of necessary conditions that only in special cases is sufficient for the obtained solution to be exactly N representable, meaning a physical $|\Psi\rangle$ to exist such that Eq. (14) holds.

The minimization of the functional (15) is performed by forming an augmented Lagrangian function and minimizing it following the algorithm in Ref. 42. The minimization is performed with limited memory quasi-Newton algorithm of MATHEMATICA and the form of the augmented Lagrangian is

$$L=F[\gamma]-\sum_i\lambda_i c_i+\sum_i c_i^2/\mu, \tag{16}$$

where λ_i are the Lagrange multipliers and $\mu>0$ is the augmentation parameter used to enforce the convergence of the constraints $c_i=0$. In the following, we first introduce the subset of applied N-representability conditions, and after that, impose the further constraints due to the fixed total angular momentum, M representability.

1. N representability

The trace condition

$$\sum_{i<j}\Gamma_{ij}^{ij}=\frac{N(N-1)}{2} \tag{17}$$

is used to fix the particle number to N.

Positivity conditions form the major part of the N-representability constraints. Consider an operator of the form $A=\Sigma_{i_1i_2,\ldots,i_k}t_{i_1i_2,\ldots,i_k}a_{i_1}a_{i_2},\ldots,a_{i_k}$. Since $\langle\Psi|A^\dagger A|\Psi\rangle\geq0$, it follows that

$$\sum_{\substack{i_1i_2,\ldots,i_k\\ j_1j_2,\ldots,j_k}} t_{i_1i_2,\ldots,i_k}^* t_{j_1j_2,\ldots,j_k}\Gamma_{j_1j_2,\ldots,j_k}^{i_1i_2,\ldots,i_k}\geq0. \tag{18}$$

For $k=2$ we obtain the two-positivity condition for the 2-RDM

$$\sum_{\substack{ij\\ kl}} t_{ij}^* t_{kl}\Gamma_{kl}^{ij}\geq0. \tag{19}$$

By a different choice of A, positivity conditions of the exact same form can be derived for the two other representations of the 2-RDM

$$Q_{kl}^{ij}=\langle\Psi|a_i a_j a_l^\dagger a_k^\dagger|\Psi\rangle$$

and

$$G_{kl}^{ij}=\langle\Psi|a_i^\dagger a_j a_l^\dagger a_k|\Psi\rangle. \tag{20}$$

While the representations Γ, Q, and G are all equivalent as they are related by the fermionic anticommutation rules, the positivity conditions are inequivalent and must be taken into account simultaneously. We use the antisymmetric basis $|(ij)\rangle=(|ij\rangle-|ji\rangle)/2$ for Γ and Q matrices since $\Gamma_{kl}^{ij}=-\Gamma_{kl}^{ji}=-\Gamma_{lk}^{ij}$ and $Q_{kl}^{ij}=-Q_{kl}^{ji}=-Q_{lk}^{ij}$. Furthermore following Ref. 42, since all the three matrices are real and symmetric under $ij\leftrightarrow kl$, the positive-definite condition can be accounted for simply by writing the matrices as square of sym-

metric matrices $\Gamma=R^2$, $Q=S^2$, and $G=T^2$ (meaning $\Gamma^{(ij)}_{(kl)}=\Sigma_{(pq)}R^{(ij)}_{(pq)}R^{(pq)}_{(kl)}$, etc.) and optimizing the upper diagonal of matrices R, S, and T. The linear relations linking Γ and Q and Γ and G become the relevant constraint equations

$$Q^{ij}_{kl}=\Gamma^{ij}_{kl}-\delta_{ik}\gamma_{jl}-\delta_{jl}\gamma_{ik}+\delta_{il}\gamma_{jk}+\delta_{jk}\gamma_{il}+\delta_{ik}\delta_{jl}-\delta_{il}\delta_{jk},$$

$$G^{ij}_{kl}=\delta_{jl}\gamma_{ik}-\Gamma^{il}_{kj}, \tag{21}$$

where the 1-RDM γ_{ij} may be obtained through

$$\sum_k G^{ij}_{kk}=N\gamma_{ij} \quad \text{or} \quad \sum_k \Gamma^{ik}_{jk}=(N-1)\gamma_{ij}. \tag{22}$$

2. M representability

Since $\Sigma_i m_i a_i^\dagger a_i|\Psi\rangle=M|\Psi\rangle$, we can form one independent nontrivial equation involving 2-RDM (equivalent to the contracted Schrödinger equation in Ref. 29)

$$\sum_k m_k G^{ij}_{kk}=M\gamma_{ij}. \tag{23}$$

The trace of this is already fixed by Eqs. (17) and (22)

$$\sum_{ij} m_j G^{ii}_{jj}=MN. \tag{24}$$

Since in our system the angular momentum quantum numbers $m_j=j$ are always non-negative, the maximum angular momentum for a pair of electrons to have is $k_2=M-(N-2)(N-3)/2$ where the subtracted term is the minimum angular momentum of $N-2$ electrons. Additionally, some of the matrix elements of the 2-RDM are zero because states with different total angular momentum are orthogonal. The independent constraints due to these considerations read

$$\Gamma^{ij}_{kl}=0, \quad i+j\neq k+l \ \text{ or } \ i+j>k_2 \tag{25}$$

while Eq. (21) communicates them to Q and G. Though we can just drop the corresponding terms from our equations, we still need to take into account the ensuing constraints on the actual variables R, S, and T.

C. Monte Carlo

The calculation of the natural orbital occupations is relatively simple using the Monte Carlo technique. Unlike in the previous Monte Carlo study in Ref. 43, we know from the start the natural orbitals that diagonalize the density matrix and thus we only need to calculate the occupations.

Starting from the definition in Eq. (2), the orthogonality of the natural orbitals, and the expansion of 1-RDM using the natural orbitals

$$\gamma(\mathbf{r},\mathbf{r}')=\sum_m n_m\phi^*_m(\mathbf{r})\phi_m(\mathbf{r}') \tag{26}$$

the occupations are integrated as

$$n_m=N\int \Psi^*(\mathbf{r}_1,\mathbf{r}_2,\ldots)\Psi(\mathbf{r}',\mathbf{r}_2,\ldots) \times \phi_m(\mathbf{r}_1)\phi^*_m(\mathbf{r}')d\mathbf{r}'d\mathbf{r}_1,\ldots,d\mathbf{r}_N. \tag{27}$$

This is further reformulated as

$$n_m=N\int |\Psi(\mathbf{r}_1,\mathbf{r}_2,\ldots)|^2\frac{\Psi(\mathbf{r}',\mathbf{r}_2,\ldots)}{\Psi(\mathbf{r}_1,\mathbf{r}_2,\ldots)} \times \phi_m(\mathbf{r}_1)\phi^*_m(\mathbf{r}')d\mathbf{r}'d\mathbf{r}_1,\ldots,d\mathbf{r}_N, \tag{28}$$

which can be symmetrized and rewritten in Monte Carlo expectation value as

$$n_m=\left\langle \sum_i \int \frac{\Psi(\mathbf{r}',\mathbf{r}_2,\ldots)}{\Psi(\mathbf{r}_1,\mathbf{r}_2,\ldots)}\phi_m(\mathbf{r}_i)\phi^*_m(\mathbf{r}')d\mathbf{r}' \right\rangle_{\{\mathbf{r}_i\}\in|\Psi|^2},$$

where the summation is over the coordinates $\{\mathbf{r}_i\}_{i=1}^N$. The first strategy for Monte Carlo evaluation of the occupation is to sample these coordinates from $|\Psi|^2$ and to integrate over $\mathbf{r}'$ on a grid.[43]

For a better option in our case, we first rewrite $\phi_m(\mathbf{r}_i)\phi^*_m(\mathbf{r}')=|\phi_m(\mathbf{r}')|^2\frac{\phi_m(\mathbf{r}_i)}{\phi_m(\mathbf{r}')}$ and then do a Monte Carlo integration also over $\mathbf{r}'$ as

$$n_m=\left\langle \sum_i \frac{\Psi(\mathbf{r}',\mathbf{r}_2,\ldots)}{\Psi(\mathbf{r}_1,\mathbf{r}_2,\ldots)}\frac{\phi_m(\mathbf{r}_i)}{\phi_m(\mathbf{r}')} \right\rangle_{\{\mathbf{r}_i\}\in|\Psi|^2,\mathbf{r}'\in|\phi_m|^2}, \tag{29}$$

where $\{\mathbf{r}_i\}_{i=1}^N$ is again sampled from $|\Psi|^2$ and $\mathbf{r}'$ from $|\phi_m|^2$. This option can be made more stable by noting that the natural orbitals have rotation symmetry and $|\phi_m(\mathbf{r}')|^2$ depends only on the radial coordinate r' and not on the angle θ'. Now, the radial integral over r' can be done using Monte Carlo integration and the angular integral by averaging over a uniform grid $\{\theta'_j\}_{j=1}^{N_{\theta'}}$ as

$$n_m=\left\langle \frac{1}{N_{\theta'}}\sum_{i,j} \frac{\Psi(\mathbf{r}',\mathbf{r}_2,\ldots)}{\Psi(\mathbf{r}_1,\mathbf{r}_2,\ldots)}\frac{\phi_m(r_i,\theta_i)}{\phi_m(r',\theta'_j)} \right\rangle_{\{\mathbf{r}_i\}\in|\Psi|^2,r'\in|\phi_m|^2}.$$

Notice that r' is generated separately for each ϕ_m.

V. RESULTS

In the following, we will first compare the performance of various 1-RDM functionals in calculating the interaction energies in different (N,M) sectors in exactly solvable small quantum Hall droplets. This analysis is deepened by analyzing the occupation numbers obtained for the ground states. Once we have established that we have a decent functional, we proceed to test its performance in larger systems. Since no exact results are available for larger systems at the strongly correlated regime $\nu\ll 1$, we employ the next best-gripping handle, which is the Laughlin's variational wave function for filling fraction $\nu=1/3$. Moreover, we compare the energies and occupations obtained with density-matrix power functionals (P-α) to the results extracted from the Laughlin's wave function with Monte Carlo techniques. From the occupation numbers we calculate the edge Green's function G_E, which gives information about the topological

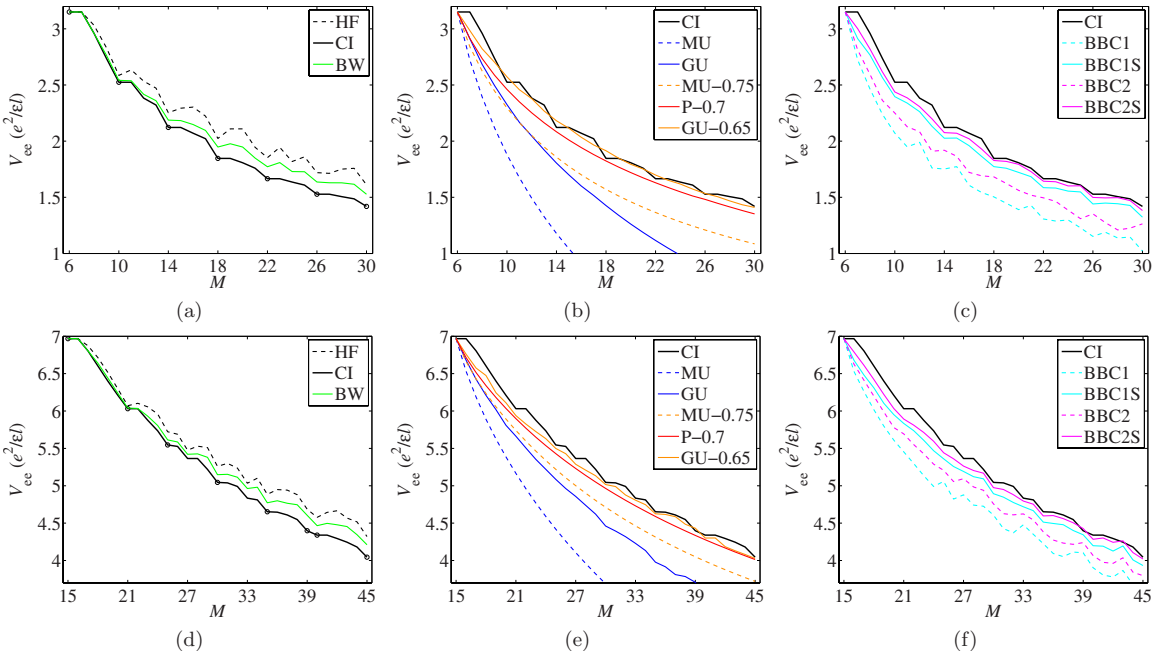

FIG. 1. (Color online) The minimum interaction energy V_{ee} at each angular momentum M for (a)–(c) four and (d)–(f) six electrons. The exact diagonalization ground states detected by the convex envelope are marked with circles in (a) and (d).

order of different quantum Hall phases. It is interesting to see if the newly applied methods (1-RDMFT and 2-RDMFT) reproduce the correct decay properties of G_E.

A. Toward a good 1-RDM functional in small quantum Hall droplets

The energy states of the quantum dot may be written as

$$E^n_{MN} = N\hbar\omega + (\hbar\omega - \hbar\omega_c/2)M + V^n_{ee}(M,N), \qquad (30)$$

where $V^n_{ee}(M,N)$ is the nth eigenvalue of the total interaction energy in sector (M,N), whose dependence on the physical parameters is scaling by a factor $e^2/\epsilon l$. Because of the second term, it follows that all possible ground states for N particles are found at the intersections of the M-V_{ee} curve and its convex lower envelope.

Figure 1(a) shows the M-V_{ee} curves for four electrons computed with the CI, HF method, and the BW second-order perturbation theory to the HF state. The exact diagonalization (CI) ground states, detected by the convex envelope, are marked by circles. While both HF and BW predict the correct ground states, the perturbation theory leads to a significant improvement to the HF energy. The second-order perturbation theory is very accurate and close to the CI result for $M<14$, and it is roughly halfway between HF and CI energy for $M>14$.

Physically the cusp structure seen in the results follows from the energetic advantage of a configuration, in which the four electrons are located at vertices of a square. This configuration has nonzero weight only if the angular momentum attains a special value such that $N(N-1)/2 \equiv \mathrm{mod}(M,N)$. The difference between subsequent magic angular momentum states is the number of vortices found at the center of the system. As magnetic field is increased, vortices that carry quantized angular momentum, and in a sense-quantized magnetic flux, emerge at the center. As the particle number is taken very large, the number of cusps increases while all cusps no longer correspond to a ground state at certain system parameters. Instead, a few of them are more special than others forming the incompressible vacuum state of certain fractional quantum Hall phase as the remaining cusps are related to the quasiparticle/vortex excitations that are eventually responsible for the finite extension of the quantum Hall plateaus.

The corresponding energies obtained with 1-RDMFT are shown in Figs. 1(b) and 1(c). At this point the choice of parameters $\alpha=0.75$, $\alpha=0.7$, and $\alpha=0.65$ for MU-α, P-α, and GU-α is an educated guess, whereas the effect of the parameter α becomes apparent in the next section (basically, it tunes the strength of electron correlations). Typical to 1-RDMFT calculations in general, the energies are below the CI result. The dashed lines systematically lie below the solid lines of the same tone due to the self-energy cancellation present in the latter. Basic MU and GU functionals clearly overestimate the correlation energy and behave even qualitatively wrong as they fall too fast with increasing M. For the rest of the functionals, V_{ee} seems to decline at about the correct rate as a function of M. However, a nice cusp structure is only seen with the BBC1S and BBC2S functionals, which inherit the cusps from the HF state used in the selection of the strongly and weakly occupied orbitals. Overall the energetically best of these 1-RDM functionals (P-0.7, GU-0.65, BBC1S, and BBC2S) perform better than the second-order perturbation theory when $M>14$, although only BBC2S produces the correct ground-state structure.

The equivalent curves for six electrons are shown in Figs. 1(d)–1(f). As the six-electron results are quantitatively like the four-electron results, the performance of different functionals seems to be rather insensitive to the particle

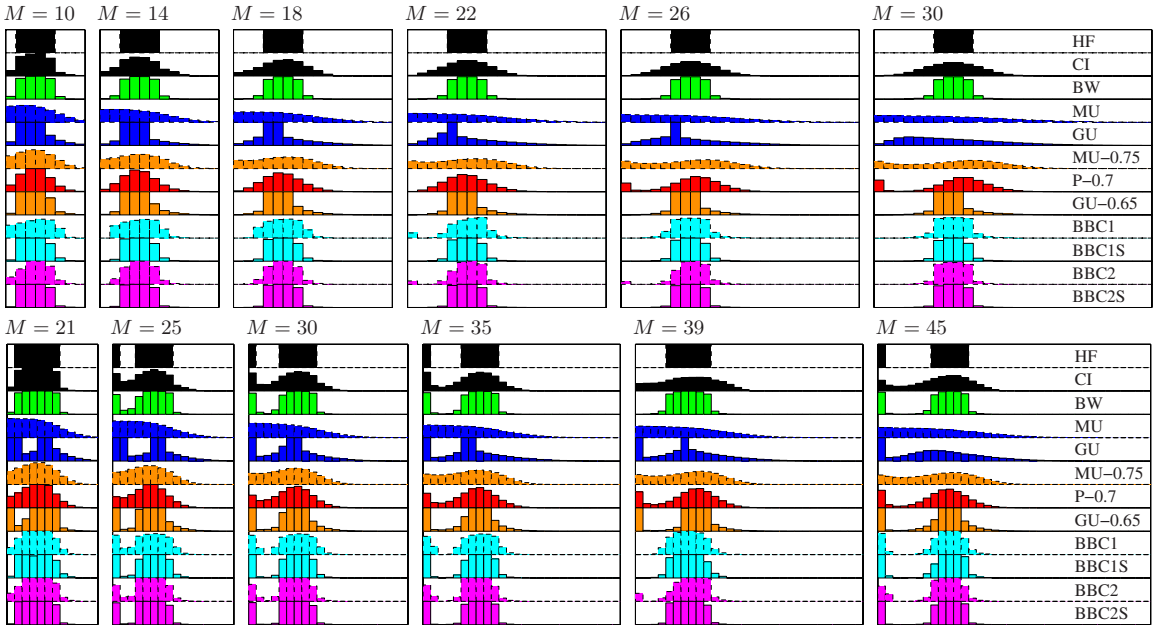

FIG. 2. (Color online) The occupation numbers for selection of the four-electron (upper panel) and six-electron (lower panel) ground states indicated in Figs. 1(a) and 1(d), respectively. A bar that fills the assigned height corresponds to occupation number 1. Occupations are ordered according to the increasing single-particle angular momentum m of the lowest Landau-level orbitals starting with 0 at the left. Because most likely location of electron at orbital m is at distance $r=\sqrt{m}$ from the center, one can think the set of orbitals as a radially discretized disk.

number. For six electrons, the cusps should occur at $N(N-1)/2 \equiv \mathrm{mod}(M,N)$ or $N(N-1)/2 \equiv \mathrm{mod}(M,N-1)$ corresponding to a hexagonal configuration or a pentagonal configuration with one electron at the center. All the cusps are not correctly reproduced with any 1-RDM functional, though BBC2S result follows the cusp structure quite well at $M>27$.

The quantum Hall droplet model has the property that an increase in M increases the area of the droplet and also the electronic correlations quantified in reduction in the occupation numbers of the natural Landau-level orbitals. The average occupation number of the relevant orbitals is close to the corresponding macroscopic quantum Hall filling fraction ν and becomes exact as N is taken to infinity. For example, the $\nu=1$ state occurs at the minimum angular momentum $M=N(N-1)/2$ where the first N orbitals have occupation 1. Second example is the Laughlin's wave function[4] for filling fraction $\nu=1/3$

$$\Psi_{\mathrm{L}}^{1/3}(\{z_i\}) = \prod_{i<j} (z_i - z_j)^3 e^{-1/2\Sigma_i z_i \bar{z}_i}. \tag{31}$$

It has angular momentum $M=3N(N-1)/2$ and $3(N-1)+1$ nonempty orbitals such that on average the fraction $\nu=N/[3(N-1)+1] \approx 1/3$ is filled. The Laughlin state has about 0.98 overlap with the exact ground state for four and six electrons, and it is the lowest angular momentum zero-energy state of the short-range model interaction[44]

$$V_1(z_{ij}) = \partial_{z_i} \partial_{\bar{z}_i} \delta(z_i - z_j) + i \leftrightarrow j. \tag{32}$$

Note, however that while for four electrons the highly correlated Laughlin state occurs at $M=18$ near the center of the M window in the M-V_{ee} curves, the corresponding angular momentum for six electrons is $M=45$, and it is the highest M included in the corresponding figures. Overall, it seems that the perturbation theory works energetically well near $\nu=1$ where the correlations are weak while the 1-RDM functionals perform better at the strongly correlated regime $\nu \ll 1$, which raises some hope for the 1-RDMFT to prove valuable in quantum Hall systems.

But how close are the obtained minimizing 1-RDMs actually to the exact results? Recall that the natural orbitals in the lowest Landau level are fixed and their occupations completely specify the 1-RDM. Figure 2 shows the occupation numbers corresponding to the ground states indicated in Figs. 1(a) and 1(d).

Looking at the first row of occupation numbers for four electrons, the next HF ground state is obtained from the previous by adding a hole to the center leading to angular momentum increase N. The exact CI result below is similar but, in addition, the correlations spread the occupations at each step. On the third row, the second-order perturbation theory BW has a small spread of occupations in accordance with the energy curves in Fig. 1(a). The 1-RDM functional results on the following nine rows are varied in nature. In accord with the poor energies, MU functional leads to a way too large spread of occupation and so does the GU although the latter also pins some occupations to one. The inclination toward pinning is due to the self-energy cancellation since without the cancellation nonpinned occupations lead to negative self-energy contribution lowering the total energy ($n_i^2 - n_i < 0$ for $0 < n_i < 1$). This is the reason why MU-0.75 is more spread out than GU-0.65, and BBC occupations are a bit less pinned than BBCS occupations. Despite the better energetics, the

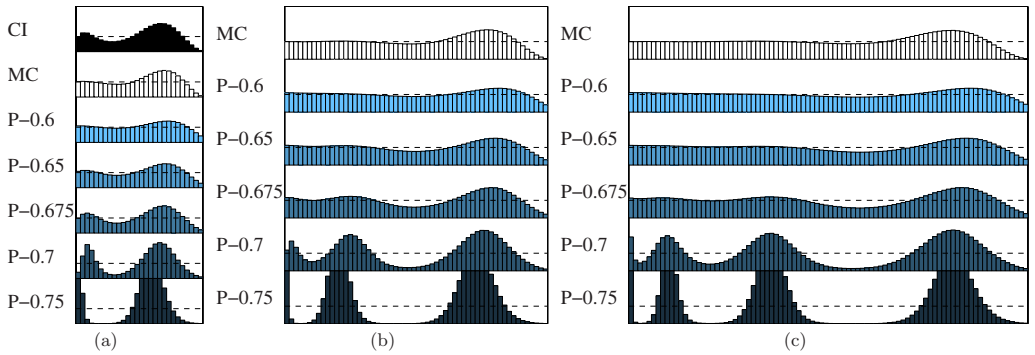

FIG. 3. (Color online) The occupation numbers at the angular momentum of the 1/3 Laughlin state for (a) $N=10$, (b) $N=20$, and (c) $N=30$ electrons with $3(N-1)+1$ natural orbitals. MC is the exact Laughlin wave-function result extracted with Monte Carlo. The dashed line marks 1/3 occupation.

GU-0.65, BBC1S, and BBC2s occupations seem not to be much better than the second-order perturbation theory. On the contrary, P-0.7, on the other hand, has both quite good energy and occupations numbers only slightly less spread than the exact result. Note however, the nonzero first occupation at $M=26$ and $M=30$ in contrast to the exact result.

For six electrons [Fig. 1 (lower)], the occupations are similar. Note the high probability for one electron to be at the center in some of the HF and CI ground states, correctly reproduced by many of the functionals. The six-electron occupation numbers at $M=30$ and $M=35$ can be directly compared to the occupations obtained with DFT in Ref. 15 and they are found to be a bit similar to our BBC1 or BBC2 results.

On the whole, the P-0.7 power functional seems like a good candidate functional for systems with large number of electrons. GU-α with $\alpha<0.65$ and MU-α with $\alpha>0.75$ could also work well, however, since the diagonal part of the P-α functional is somewhat a compromise between these two, we employ the P-α functional in the remainder of the manuscript.

B. 1-RDM *at large N*

The results of the previous section suggest that the density-matrix power functional (P-α) could be a good functional in quantum Hall systems and thus we apply it to large systems for a few parameters α. Moreover, we concentrate on the $\nu=1/3$ state, whereby close to exact nonperturbative results can be computed with the Laughlin's variational wave function [Eq. (31)] using Monte Carlo. It is natural to limit the number of natural orbitals to that of the Laughlin wave function $3(N-1)+1$ although the realistic Coulomb ground state would actually extend, weakly though, to a few more orbitals.

The occupation numbers obtained in such way for $N=10$, $N=20$, and $N=30$ are presented in Fig. 3. As seen in the exact result [first row in Fig. 3(a)] the long-range Coulomb correlations cause oscillations in the occupations around 1/3 (CI), apart from the edge density modulation not present in the Laughlin's occupation numbers (MC). Sliding α from 0.6 to 0.75 gradually strengthens these oscillations. P-0.65 is close to the Laughlin's occupations while P-0.675 is close to the exact occupations (CI). Similar behavior is seen at larger particle numbers in Figs. 3(b) and 3(c), where P-0.675 yields again occupations plausibly closest to the exact unknown result.

The oscillations in the occupation numbers reflect the formation of an edge striped phase. An extrapolated phenomenological formula for the slow-decaying charge-density oscillations at the $\nu=1/3$ edge at the thermodynamic limit is given in Ref. 25

$$\rho(s)=\frac{1}{6}[\mathrm{Erf}(s)+1]\left\{1+\frac{1}{2}J_0\left[\frac{\pi}{2}(s-1)\right]\right\}, \tag{33}$$

where $s/\sqrt{2}$ is the distance from the edge located at $\sqrt{3(N-1)}$, Erf is the Gauss error function, and J_0 is the Bessel function of the first kind. Figure 4(a) shows the radial charge densities $\langle\Psi|\psi^\dagger(r)\psi(r)|\Psi\rangle$ calculated from the 30 electron occupation numbers compared to the extrapolated formula red (dark gray) dashed line. The latter has slightly longer oscillation wavelength compared to the P-α results while the amplitude of oscillations suggests that the optimal value of α is somewhere between 0.675 and 0.7. Thus, although Eq. (33) has zero free parameters, it matches the 1-RDM results reasonably well.

Edge Green's function G_E is the amplitude for electron to propagate a distance along the edge. In the quantum Hall droplet, the distance is related to the angle θ between the two points, and $G_\mathrm{E}=\langle\Psi|\psi^\dagger(z_0e^{i\theta})\psi(z_0)|\Psi\rangle$, where z_0 is a point of the edge. Chiral Luttinger-liquid theory of the fractional quantum Hall edge predicts the universal asymptotic behavior[9,10]

$$|G_\mathrm{E}|\propto|z_0e^{i\theta}-z_0|^{-g}\propto|\sin(\theta/2)|^{-g}, \tag{34}$$

where $g=3$ for $\nu=1/3$. Values of $g\neq1$ lead to non-Ohmic current-voltage dependence $I\propto V^g$ in the tunneling experiments. However, thus observed experimental value, $g\approx2.2-2.8$, is contrary to the theory possibly sample dependent.[26,27]

The decay of $|G_\mathrm{E}|$ calculated with the density-matrix power functionals is compared to the exact (CI) and the Laughlin wave function's result (MC) in Figs. 4(b) and 4(c) for $N=10$ and $N=20$, respectively (not shown case $N=30$ looks similar). The short lines signify power-law exponents

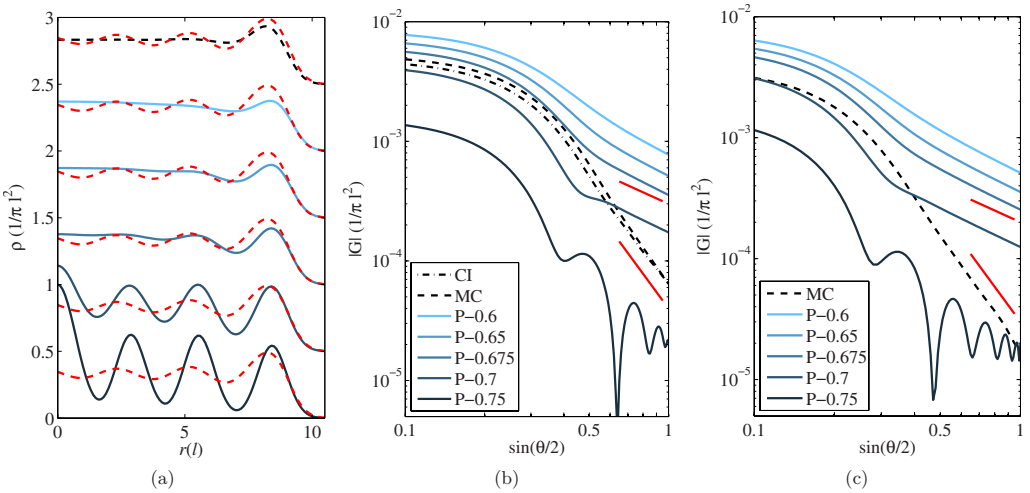

FIG. 4. (Color online) (a) 30 electron-density profiles corresponding to Fig. 3(c) shifted vertically by 0.5 unit. Red (dark gray) dashed line is the phenomenological estimate for the density oscillations at the thermodynamic limit. [(b) and (c)] The decay of the edge Green's function calculated at $r=\sqrt{3(N-1)}+1$ from the occupations in Figs. 3(a) and 3(b), respectively. The short red lines illustrate slopes −3 (theoretical prediction for $\nu=1/3$) and −1 (Fermi liquid).

$g=1$ and $g=3$. Except for the curve corresponding to P-0.75, which oscillates heavily, the P-α curves follow closely the theoretical dashed black line until $\sin(\theta/2)\approx 0.3$, after which they sheer off the course to yield an exponent 1. This is due to the incorrect weights of the occupation numbers near the edge of the system and investigated further in the next section where we apply 2-RDMFT to a smaller system.

The interaction energies are shown in Table II. The exactness of the Laughlin trial wave function's energy (MC) up to 0.1% for $N=10$ is expected to carry on to the larger electron numbers. The interaction energy is seen to increase as a function of α in P-α and is optimal with the functional P-0.7, which attains 99.9% of the interaction energy for $N=20$ and 30. Typical to 1-RDMFT calculations, in general, the energies are mostly below the assumed nearly exact Monte Carlo energy.

While knowledge of the ground-state energy may be useful when comparing different methods, only energy differences are physically meaningful. In the RDM methods, we can calculate the energy differences between lowest energy states of different (M,N) sectors such as addition energy (change in N) as well as quasiparticle and some edge excitations (M changes). If the excited state becomes the ground state for some parameters, the Gilbert's theorem guarantees the existence of a 1-RDM functional minimized by the exact 1-RDM but even if this is not the case, a good functional might still exist.

TABLE II. Interaction energy in units of $e^2/\epsilon l$ at angular momentum $M=3N(N-1)/2$ and the percentage captured of the energy of the Laughlin wave function for density-matrix power functionals P-α.

	$N=10$	$N=20$	$N=30$	$N=10$ (%)	$N=20$ (%)	$N=30$ (%)
CI	10.14			99.9		
MC	10.15	32.92	64.00	100.0	100.0	100.0
P-0.6	8.93	30.36	60.08	88.0	92.2	93.9
P-0.65	9.58	31.72	62.15	94.4	96.4	97.1
P-0.675	9.87	32.34	63.10	97.2	98.2	98.6
P-0.7	10.12	32.88	63.93	99.7	99.9	99.9
P-0.75	10.44	33.44	64.80	102.9	101.6	101.2

As mentioned previously, some of the cusps in M-V_{ee} curves correspond to the quasiparticle excitations of stable quantum Hall phases. Next, we consider such a quasihole excitation above the $\nu=1/3$ state. The quasihole is a charged vortex carrying fractional charge $q=e/3$ and obeying anyonic statistics.[45,46] To obtain interaction part of the quasihole excitation energy at $\nu=1/3$, we need to calculate the difference $V_{ee}(M_{1/3}+N,N)-V_{ee}(M_{1/3},N)$. The angular momentum $M_{1/3}+N$ follows from the Laughlin's quasihole wave function, which is also used to compute an estimate for $V_{ee}(M_{1/3}+N,N)$ with Monte Carlo. Due to the fact that Laughlin's wave function is more accurate than the quasihole wave function, variational principle implies that the Monte Carlo estimate to the (negative) contribution to the excitation energy is likely an upper bound to the exact result. Nevertheless, for eight particles the difference to exact CI result is less than 0.2% so we expect the estimates to be quite accurate. The quasihole wave function reads

$$\Psi_{\mathrm{L}}^{1/3}(\{z_i\})=\prod_i (z_i-z_{\mathrm{CM}})\prod_{i<j}(z_i-z_j)^3 e^{-1/2\Sigma_i z_i\bar{z}_i}, \qquad (35)$$

where $z_{\mathrm{CM}}=(1/N)\Sigma_i z_i$. The interaction contribution to the excitation energy is shown in Table III. The power functionals appear to overestimate the energy gap by 10–20 % compared to the trial wave function though the results seem to get more accurate with increasing N. This preliminary result indicates that the method could prove useful in assessing the stability of different models for quantum Hall phases characterized by certain angular momentum and spin. Additionally, 1-RDM method offers a simple framework to include the higher Landau levels, however, instead of the bare eigenval-

TABLE III. Interaction energy of one elementary quasihole excitation in units of $e^2/\epsilon l$ and the percentage captured of the interaction energy of the wave functional quasihole model (MC).

	$N=10$	$N=20$	$N=30$	$N=10$ (%)	$N=20$ (%)	$N=30$ (%)
MC	−0.314	−0.497	−0.635	100	100	100
P-0.6	−0.396	−0.601	−0.758	126	121	119
P-0.65	−0.381	−0.588	−0.736	121	118	116
P-0.675	−0.376	−0.583	−0.733	120	117	115
P-0.7	−0.376	−0.584	−0.689	120	118	109
P-0.75	−0.378	−0.585	−0.326	120	118	51

ues of the reduced density matrix, one must then optimize the eigenvectors also.

C. 2-RDMFT results for three electrons

In this final part, we apply the exact 2-RDM functional [Eq. (3)] to a three electron droplet in the 1/3 state again with the maximum single-particle angular momentum set to $3(N-1)$. We will see that the resulting 2-RDM, though not strictly physical, is close to the exact solution and yields better results than our 1-RDM functionals.

Compared to the 1-RDM calculations seen above, the computational cost of the problem in the 2-RDM optimization is considerably larger and scales at higher order p^6 (versus p^4) with the number of single-particle orbitals p. The 1/3 Laughlin state for three electrons has angular momentum $M=9$ and requires only seven single-particle states. However, the number of optimization variables in Γ, Q, and G are 276, 378, and 1225, respectively, and the constraint Eqs. (17), (21), (23), and (25) together lead to 2798 constraints each facilitated by a Lagrange multiplier. In practice, this means that this method takes more time than exact diagonalization in any system that could be solved in a reasonable time. However, owing to the exponential scaling of the exact diagonalization problem, the situation could change in future with development of faster computers and more efficient semidefinite programming and optimization algorithms.

Figure 5 shows the occupation numbers and the decay of the edge Green's function for three electrons at $\nu=1/3$ $[M=3N(N-1)/2=9]$. Due to a finite-size effect, the exact diagonalization Green's function has a downward cusp at $\sin(\theta/2)\approx 0.9$. The 2-RDMFT result has a similar cusp while the P-0.675 result, which turns smoothly to a lower slope decay, does not have one. We verified that this is due to the difference in the weights of the last three occupation numbers corresponding to the edge of the system. Since the HF solution would have exponent $g=1$, the correct decay property of the Green's function follows from the off-diagonal terms of the interaction operator. The 1-RDMFT that only uses the diagonal V_{ijij} and V_{ijji} terms of the interaction matrix cannot yield the correct behavior unless we have a very good density-matrix functional.

Recall that the backbone of the 1-RDMFT was the approximation of the pair density. Figure 5 shows the pair-correlation functions corresponding again to exact diagonalization, 2-RDMFT, and P-0.675, where the latter is reconstructed from the 1-RDM using Eq. (4). Although the 1-RDM reconstructed pair-correlation function is reasonable vanishing at the position of the fixed electron, only the 2-RDMFT is able to produce the two-peak structure of the exact result with reduced density along the y axis (Fig. 6).

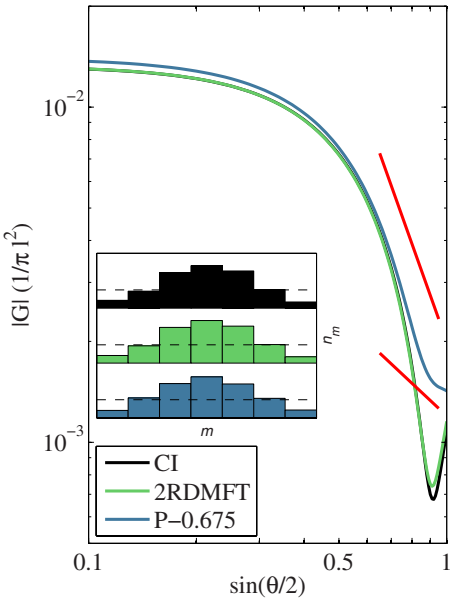

FIG. 5. (Color online) The decay of the edge Green's function corresponding to the inset three-electron occupation numbers. As previously, the short red lines illustrate slopes $-g=-3$ and -1, and G_E is evaluated at $r=\sqrt{3(N-1)}+1$.

Granted that the interaction energy functional in the 2-RDMFT is exact, the results still do not coincide with the exact diagonalization results because the three-representability conditions that ensure the physicality in this three-electron system cannot be taken into account without invoking the generalization of 2-RDMFT to include higher-order RDMs. Figure 7(a) shows the exact nonzero matrix elements of the 2-RDM $\Gamma^{(ij)}_{(kl)}$ in the antisymmetric basis $|(ij)\rangle=(|ij\rangle-|ji\rangle)/2$ and (b) calculated with the 2-RDMFT. The largest discrepancy between the results is the vanishing of the matrix elements involving states $|(14)\rangle$ or $|(25)\rangle$ for the

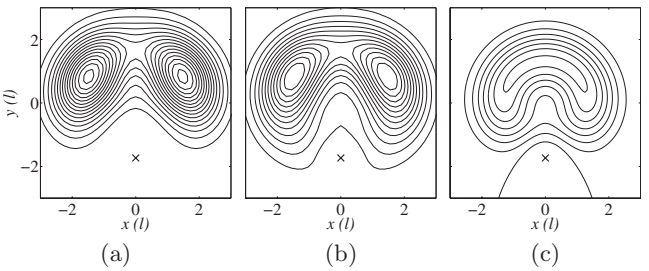

FIG. 6. The pair-correlation function $g(z_1,z_2)=\rho_2(z_1,z_2)/\rho(z_1)$ with the first coordinate placed at the density maximum of the negative y axis $z_1=-i\sqrt{3}$ for (a) exact diagonalization, (b) 2-RDMFT, and (c) 1-RDMFT with P-0.675. Contours are separated by $0.05\ 1/\pi l^2$ and start from $0.05\ 1/\pi l^2$ in (a) and (b) and from 0 in (c).

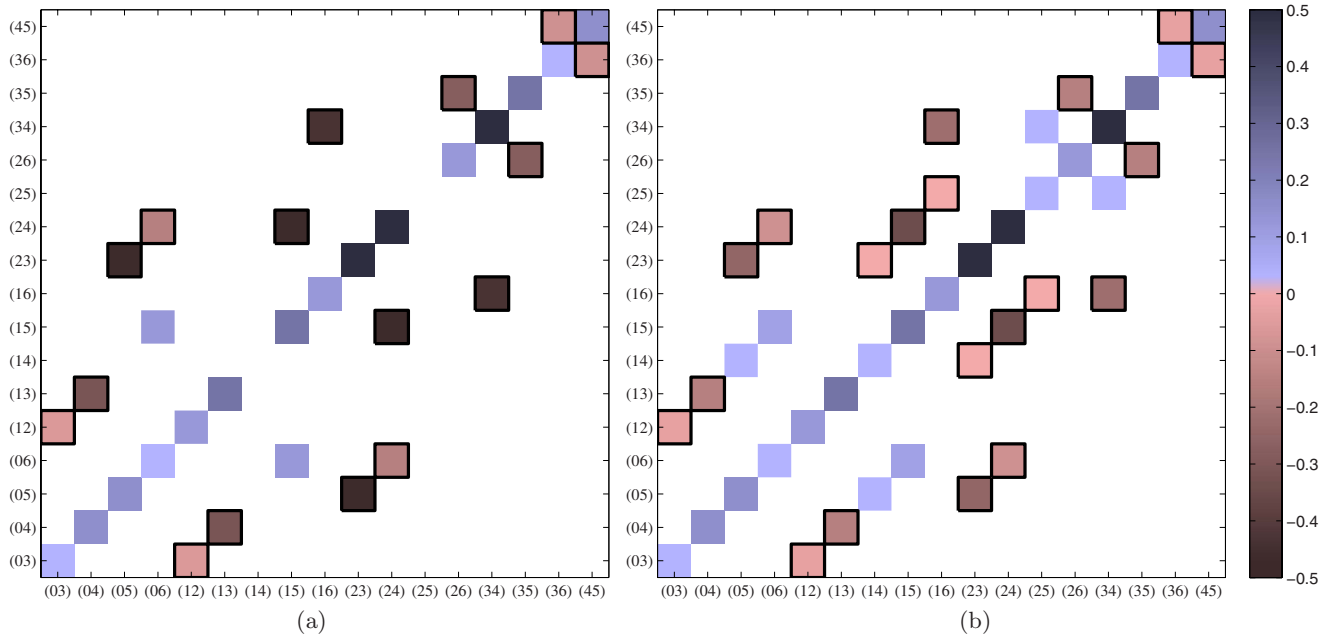

FIG. 7. (Color online) Illustration of the 2-RDM $\Gamma^{(ij)}_{(kl)}$ for three electrons in the $\nu=1/3$ state computed with (a) exact diagonalization and (b) 2-RDMFT. The same color bar applies to both figures while zero values are left white. The negative matrix elements are indicated by black edge.

exact result while for example $\Gamma^{(05)}_{(14)} \neq 0$ in the 2-RDMFT result. The matrix elements should vanish, as they are related to the fictitious many-body basis states that have double occupancy of orbital 4 or 2 (1+4+4=2+2+5=9, the total angular momentum). Consequently, the absolute values of the matrix elements also differ. However, the computed pair-correlation function and edge Green's function suggest that many of the physical quantities are not significantly affected by the absence of exact N representability and that the lack of computer power might be the only real stumbling stone in the way of the 2-RDMFT.

VI. CONCLUSIONS

In summary, we have applied the one-body reduced density-matrix functional theory to small and large quantum Hall droplets at the spin-polarized strong magnetic field regime. The density-matrix power functional seems to work reasonably well at the strongly correlated $\nu \ll 1$ regime where the occupation numbers of the natural orbitals are small. The newly applied method yields previously inaccessible valuable information with large particle numbers about the energetics and quantities that derive from the one-body reduced density matrix. The density-matrix power functional yields reasonable bulk densities with the power parameter in the range 0.65–0.7. However, the detailed properties of the edge are not produced accurately with this functional. Moreover, it is not known if a good functional for a specific quantum Hall state would work universally at different filling fractions. Nevertheless, the computationally expensive two-body reduced density-matrix method seems to facilitate the properties of the edge, though this should be verified with a larger electron number in future.

Prospects of the 1-RDMFT in quantum Hall systems include generalizations to spin and multiple Landau levels. Studies with systems without edge (sphere) and nontrivial topology (torus) are also encouraged while new state of the art energy functionals are of course very welcome.

ACKNOWLEDGMENTS

This study has been supported by the Academy of Finland through its Centres of Excellence Program (2006-2011). E.T. acknowledges financial support from the Vilho, Yrjö, and Kalle Väisälä Foundation of the Finnish Academy of Science and Letters. We also thank I. Makkonen for careful reading of the manuscript and E. Räsänen and R. van Leeuwen for useful discussions.

[1] K. v. Klitzing, G. Dorda, and M. Pepper, Phys. Rev. Lett. **45**, 494 (1980).
[2] D. C. Tsui, H. L. Stormer, and A. C. Gossard, Phys. Rev. Lett. **48**, 1559 (1982).
[3] R. B. Laughlin, Phys. Rev. B **23**, 5632 (1981).
[4] R. B. Laughlin, Phys. Rev. Lett. **50**, 1395 (1983).
[5] B. I. Halperin, Phys. Rev. B **25**, 2185 (1982).
[6] B. I. Halperin, Phys. Rev. Lett. **52**, 1583 (1984).
[7] F. D. M. Haldane, Phys. Rev. Lett. **51**, 605 (1983).
[8] J. K. Jain, Phys. Rev. Lett. **63**, 199 (1989).

[9] X. G. Wen, Int. J. Mod. Phys. B **6**, 1711 (1992).
[10] X. G. Wen, Y. S. Wu, and Y. Hatsugai, Nucl. Phys. B **422**, 476 (1994).
[11] C. Nayak, S. H. Simon, A. Stern, M. Freedman, and S. Das Sarma, Rev. Mod. Phys. **80**, 1083 (2008).
[12] A. Harju, J. Low Temp. Phys. **140**, 181 (2005).
[13] O. Heinonen, M. I. Lubin, and M. D. Johnson, Phys. Rev. Lett. **75**, 4110 (1995).
[14] S. M. Reimann and M. Manninen, Rev. Mod. Phys. **74**, 1283 (2002).
[15] H. Saarikoski, A. Harju, M. J. Puska, and R. M. Nieminen, Phys. Rev. Lett. **93**, 116802 (2004).
[16] N. Shibata and D. Yoshioka, Phys. Rev. Lett. **86**, 5755 (2001).
[17] A. E. Feiguin, E. Rezayi, C. Nayak, and S. Das Sarma, Phys. Rev. Lett. **100**, 166803 (2008).
[18] A. M. K. Müller, Phys. Lett. A **105**, 446 (1984).
[19] P. Ziesche and F. Tasnádi, Int. J. Quantum Chem. **100**, 495 (2004).
[20] M. A. Buijse, Ph.D. thesis, Vrije Universiteit, 1991.
[21] E. J. Baerends, Phys. Rev. Lett. **87**, 133004 (2001).
[22] O. Gritsenko, K. Pernal, and E. J. Baerends, J. Chem. Phys. **122**, 204102 (2005).
[23] N. N. Lathiotakis, N. Helbig, and E. K. U. Gross, Phys. Rev. B **75**, 195120 (2007).
[24] N. N. Lathiotakis, S. Sharma, J. K. Dewhurst, F. G. Eich, M. A. L. Marques, and E. K. U. Gross, Phys. Rev. A **79**, 040501(R) (2009).
[25] E. V. Tsiper and V. J. Goldman, Phys. Rev. B **64**, 165311 (2001).
[26] A. M. Chang, Rev. Mod. Phys. **75**, 1449 (2003).
[27] M. Grayson, Solid State Commun. **140**, 66 (2006).
[28] C. Garrod and J. K. Percus, J. Math. Phys. **5**, 1756 (1964).
[29] A. E. Rothman and D. A. Mazziotti, Phys. Rev. A **78**, 032510 (2008).
[30] T. L. Gilbert, Phys. Rev. B **12**, 2111 (1975).
[31] J. M. Herbert and J. E. Harriman, Int. J. Quantum Chem. **90**, 355 (2002).
[32] P. Mori-Sánchez, A. J. Cohen, and W. Yang, Phys. Rev. Lett. **102**, 066403 (2009).
[33] P. Gori-Giorgi, M. Seidl, and G. Vignale, Phys. Rev. Lett. **103**, 166402 (2009).
[34] E. Tölö and A. Harju, Phys. Rev. B **79**, 075301 (2009).
[35] E. Tölö and A. Harju, Phys. Rev. B **80**, 045303 (2009).
[36] H. Saarikoski, E. Tölö, A. Harju, and E. Räsänen, Phys. Rev. B **78**, 195321 (2008).
[37] A. Harju, S. Siljamäki, and R. M. Nieminen, Phys. Rev. B **60**, 1807 (1999).
[38] E. V. Tsiper, J. Math. Phys. **43**, 1664 (2002).
[39] MATHEMATICA is a program published by Wolfram Research Inc.
[40] S. Goedecker and C. J. Umrigar, Phys. Rev. Lett. **81**, 866 (1998).
[41] A. Coleman, Rev. Mod. Phys. **35**, 668 (1963).
[42] D. A. Mazziotti, Phys. Rev. Lett. **93**, 213001 (2004).
[43] P. R. C. Kent, R. Q. Hood, M. D. Towler, R. J. Needs, and G. Rajagopal, Phys. Rev. B **57**, 15293 (1998).
[44] S. A. Trugman and S. Kivelson, Phys. Rev. B **31**, 5280 (1985).
[45] D. Arovas, J. R. Schrieffer, and F. Wilczek, Phys. Rev. Lett. **53**, 722 (1984).
[46] F. E. Camino, Wei Zhou, and V. J. Goldman, Phys. Rev. Lett. **98**, 076805 (2007).